2

Dislocation Models of Strike-Slip Faults

In this chapter, we will begin by considering a simple two-dimensional model of a very long strike-slip fault (figure 2.1). We consider a homogeneous, linear elastic half-space. The fault is taken to be infinitely long in the x_3 direction, and the deformation is antiplane strain. This means that the only nonzero displacement is parallel to the fault in the x_3 direction, and it varies only in the plane perpendicular to the fault. That is, u_3 varies only with x_1 and x_2, $\mathbf{u}(\mathbf{x}) = u_3(x_1, x_2)\hat{\mathbf{e}}_3$. As a starting point, we will consider the slip to be uniform with depth along the fault. Later, we will consider the more realistic situation in which the slip varies with depth.

2.1 Full-Space Solution

We will begin by ignoring the earth's surface and considering a fault in a full-space. The solution for a half-space is then rather easily constructed. Notice from figure 2.1 that the displacement field is discontinuous across the fault surface; the x_2, x_3 plane. A surface of imposed displacement discontinuity is known as a *dislocation*. In the antiplane geometry, the displacement traces a helical motion around the dislocation (figure 2.2), which is therefore known as a *screw dislocation*. The line parallel to the x_3 direction where the displacement jumps discontinuously from zero to some value s is the *dislocation line*. The half-plane of the fault, $x_1 = 0$, $x_2 > 0$, is the *dislocation surface*.

The boundary condition at the dislocation is that the displacement discontinuity across the dislocation surface is equal to the fault slip, s. Adopting a radial coordinate system centered on the dislocation line (the x_3 axis),

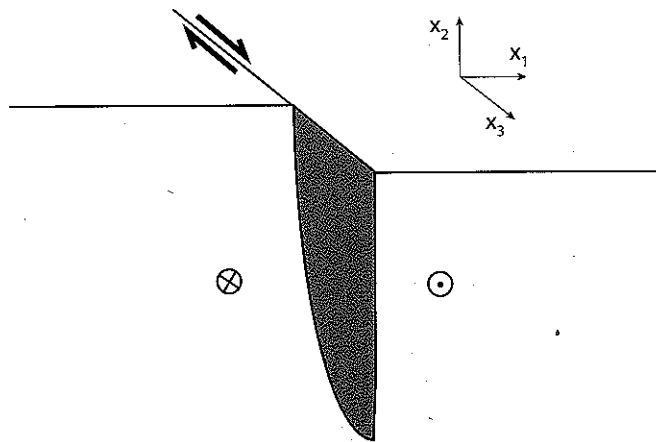$$u_3(\theta = 2\pi) - u_3(\theta = 0) = s. \tag{2.1}$$

Figure 2.1. Infinitely long strike-slip fault. The fault lies in the plane normal to x_1, with slip in the x_3 direction. The earth's surface is the plane $x_2 = 0$. In this illustration, slip tapers with depth. This chapter begins with the case in which slip is uniform with depth.
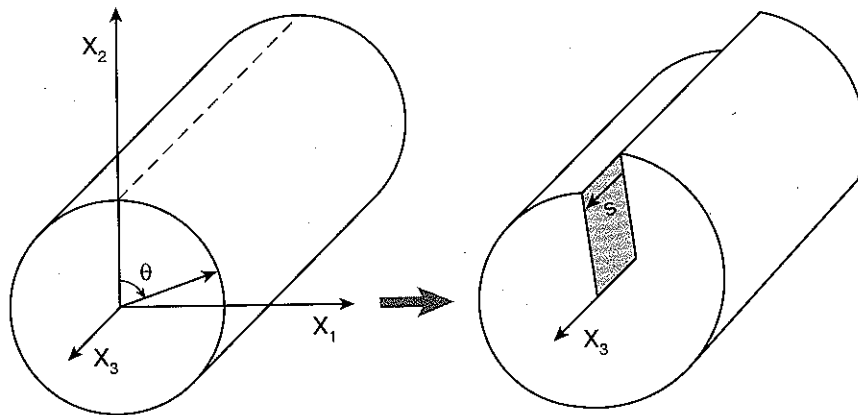
Figure 2.2. Screw dislocation, with dislocation line along x_3. The slip vector s shows the displacement of the back surface with respect to the front; the indicated slip is left-lateral.

In antiplane strain, there are only two nonzero strains, which from equations (1.4) are

$$\epsilon_{13} = \frac{1}{2}\frac{\partial u_3}{\partial x_1},$$

$$\epsilon_{23} = \frac{1}{2}\frac{\partial u_3}{\partial x_2}. \tag{2.2}$$

Hooke's law for a homogeneous, isotropic elastic material (1.103) is

$$\sigma_{ij} = 2\mu\epsilon_{ij} + \lambda\epsilon_{kk}\delta_{ij}. \tag{2.3}$$

In the antiplane case, there are only two nonzero stresses, corresponding to the shear strains (2.2):

$$\sigma_{13} = \mu\frac{\partial u_3}{\partial x_1},$$

$$\sigma_{23} = \mu\frac{\partial u_3}{\partial x_2}. \tag{2.4}$$

The stresses must satisfy the equilibrium equations (1.97). Neglecting inertial terms—that is, equivalent to assuming that the displacements develop slowly compared to elastic wave speeds—and body forces f_i, including gravity, we have

$$\frac{\partial \sigma_{ij}}{\partial x_j} = 0. \tag{2.5}$$

While in general there are three equilibrium equations, in the antiplane case, two are solved automatically, and there is only one nontrivial equation:

$$\frac{\partial \sigma_{31}}{\partial x_1} + \frac{\partial \sigma_{32}}{\partial x_2} = 0. \tag{2.6}$$

Substituting the stresses (2.4) into the equilibrium equation (2.6) yields

$$\frac{\partial^2 u_3}{\partial x_1^2} + \frac{\partial^2 u_3}{\partial x_2^2} = \boxed{\nabla^2 u_3(x_1, x_2) = 0.} \tag{2.7}$$

The displacement field satisfies Laplace's equation. This is a general result for antiplane elasticity problems. Note that since the solution is written in terms of the displacement, it is not necessary to introduce the compatibility equations.

From figure 2.2, we notice that the displacement increases smoothly with θ except at the dislocation surface. Thus, one might guess a solution of the form

$$u_3 = \pm \frac{s\theta}{2\pi}. \tag{2.8}$$

Note from equation (2.8) that u_3 increments by $\pm s$, as θ varies from 0 to 2π. In the following, we will adopt the $-s$ solution, making the sense of slip opposite to that shown in figure 2.2. Changing the sign of s simply reverses the sense of slip. For equation (2.8) to be a valid solution, it must match the boundary conditions and satisfy the equilibrium equations. Equation (2.8) was in fact constructed to satisfy the boundary condition (2.1). To see whether it also satisfies the equilibrium equations, write Laplace's equation in polar coordinates:

$$\nabla^2 u_3 = \frac{\partial^2 u_3}{\partial r^2} + \frac{1}{r}\frac{\partial u_3}{\partial r} + \frac{1}{r^2}\frac{\partial^2 u_3}{\partial \theta^2}. \tag{2.9}$$

In this form, it is clear that $\nabla^2 u_3 = 0$. Thus, equation (2.8) satisfies the governing equation and the slip boundary condition on the fault surface. If we had not recalled the Laplacian in polar coordinates, we could also check that equation (2.8) satisfies equation (2.7) by converting the displacements to Cartesian coordinates:

$$u_3 = -\frac{s\theta}{2\pi} = -\frac{s}{2\pi}\tan^{-1}\left(\frac{x_1}{x_2}\right). \tag{2.10}$$

The relevant partial derivatives are

$$\frac{\partial u_3}{\partial x_1} = -\frac{s}{2\pi}\frac{x_2}{x_1^2 + x_2^2},$$

$$\frac{\partial u_3}{\partial x_2} = \frac{s}{2\pi}\frac{x_1}{x_1^2 + x_2^2}. \tag{2.11}$$

A further differentiation of equation (2.11) verifies that the equilibrium equations are indeed satisfied.

Solution (2.8) satisfies equilibrium and the boundary conditions on the dislocation surface. What about the stress far from the dislocation—that is, as $r \to \infty$? The stresses can be found from equations (2.4) and (2.11):

$$\sigma_{23} = \mu\frac{\partial u_3}{\partial x_2} = \frac{s\mu}{2\pi}\frac{x_1}{x_1^2 + x_2^2} = \frac{s\mu}{2\pi}\frac{\sin\theta}{r}, \tag{2.12}$$

$$\sigma_{13} = \mu\frac{\partial u_3}{\partial x_1} = \frac{-s\mu}{2\pi}\frac{x_2}{x_1^2 + x_2^2} = \frac{-s\mu}{2\pi}\frac{\cos\theta}{r}. \tag{2.13}$$
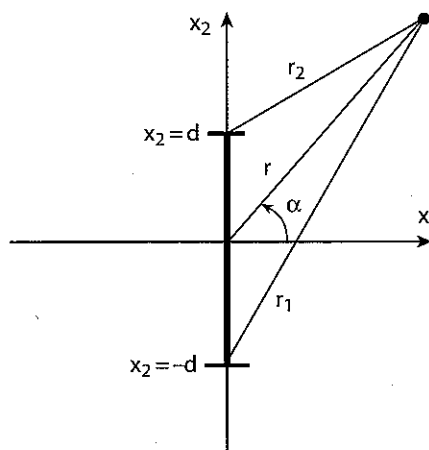
Figure 2.3. Dislocation dipole. A pair of oppositely signed dislocations are located at $x_2 = -d$ and $x_2 = +d$, causing uniform slip in the enclosed interval.

Notice that the stresses decay as $1/r$ from the *dislocation line*, not the dislocation surface. It is the dislocation line that is the source of strain, not the dislocation surface.

We will next consider slip extending over a finite interval in the x_2 direction. This solution is easily obtained summing the solutions for two oppositely signed dislocations. The governing differential equation (2.7) is linear. Thus, if two displacement fields $u^{(1)}$ and $u^{(2)}$ independently solve equation (2.7)—that is, $\nabla^2 u^{(1)} = 0$ and $\nabla^2 u^{(2)} = 0$—their sum also satisfies the equation $\nabla^2(u^{(1)} + u^{(2)}) = 0$. This is known as the *principle of superposition*. In particular, add a screw dislocation at depth $x_2 = -d$ and an oppositely signed screw dislocation at depth $x_2 = +d$ (figure 2.3). A dislocation at $x_2 = d$ is obtained by replacing x_2 with $x_2 - d$ in equation (2.10). This leads to

$$u_3 = \frac{-s}{2\pi} \left[\tan^{-1}\left(\frac{x_1}{x_2 + d}\right) - \tan^{-1}\left(\frac{x_1}{x_2 - d}\right) \right] . \qquad (2.14)$$

The stress due to slip over the finite interval is thus

$$\sigma_{13} = \frac{-s\mu}{2\pi} \left(\frac{x_2 + d}{r_1^2} - \frac{x_2 - d}{r_2^2} \right) , \qquad (2.15)$$

where the distance from the lower dislocation is $r_1^2 = x_1^2 + (x_2 + d)^2$, and the distance from the upper dislocation is $r_2^2 = x_1^2 + (x_2 - d)^2$. On the plane of the fault, $x_1 = 0$, this becomes

$$\sigma_{13}(x_1 = 0) = \frac{s\mu d}{\pi(x_2^2 - d^2)} = \frac{s\mu d}{\pi(x_2 - d)(x_2 + d)} \qquad (2.16)$$

(see figure 2.4). Note that equation (2.16) gives the change in stress due to slip on the fault. The total stress is the sum of any preexisting stresses and the changes due to fault slip. As expected, the stress change is negative inside the slipping zone and positive outside this region. We interpret the negative stress as a decrease relative to some initial state and the positive stresses as a stress increase. Physically, it makes sense for fault slip to relax the stress. Because the slip changes discontinuously from s to 0, the strains, and thus stresses, are infinite at the dislocation line. Note from equations (2.12) and (2.13) that the dislocation stresses have a $1/r$
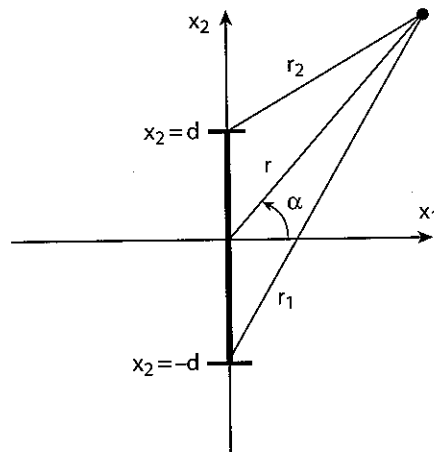
Figure 2.3. Dislocation dipole. A pair of oppositely signed dislocations are located at $x_2 = -d$ and $x_2 = +d$, causing uniform slip in the enclosed interval.

Notice that the stresses decay as $1/r$ from the *dislocation line*, not the dislocation surface. It is the dislocation line that is the source of strain, not the dislocation surface.

We will next consider slip extending over a finite interval in the x_2 direction. This solution is easily obtained summing the solutions for two oppositely signed dislocations. The governing differential equation (2.7) is linear. Thus, if two displacement fields $u^{(1)}$ and $u^{(2)}$ independently solve equation (2.7)—that is, $\nabla^2 u^{(1)} = 0$ and $\nabla^2 u^{(2)} = 0$—their sum also satisfies the equation $\nabla^2(u^{(1)} + u^{(2)}) = 0$. This is known as the *principle of superposition*. In particular, add a screw dislocation at depth $x_2 = -d$ and an oppositely signed screw dislocation at depth $x_2 = +d$ (figure 2.3). A dislocation at $x_2 = d$ is obtained by replacing x_2 with $x_2 - d$ in equation (2.10). This leads to

$$u_3 = \frac{-s}{2\pi} \left[\tan^{-1}\left(\frac{x_1}{x_2 + d}\right) - \tan^{-1}\left(\frac{x_1}{x_2 - d}\right) \right]. \tag{2.14}$$

The stress due to slip over the finite interval is thus

$$\sigma_{13} = \frac{-s\mu}{2\pi} \left(\frac{x_2 + d}{r_1^2} - \frac{x_2 - d}{r_2^2} \right), \tag{2.15}$$

where the distance from the lower dislocation is $r_1^2 = x_1^2 + (x_2 + d)^2$, and the distance from the upper dislocation is $r_2^2 = x_1^2 + (x_2 - d)^2$. On the plane of the fault, $x_1 = 0$, this becomes

$$\sigma_{13}(x_1 = 0) = \frac{s\mu d}{\pi(x_2^2 - d^2)} = \frac{s\mu d}{\pi(x_2 - d)(x_2 + d)} \tag{2.16}$$

(see figure 2.4). Note that equation (2.16) gives the change in stress due to slip on the fault. The total stress is the sum of any preexisting stresses and the changes due to fault slip. As expected, the stress change is negative inside the slipping zone and positive outside this region. We interpret the negative stress as a decrease relative to some initial state and the positive stresses as a stress increase. Physically, it makes sense for fault slip to relax the stress. Because the slip changes discontinuously from s to 0, the strains, and thus stresses, are infinite at the dislocation line. Note from equations (2.12) and (2.13) that the dislocation stresses have a $1/r$

(2.7)

t for antiplane
isplacement, it

θ except at the

(2.8)

the following,
n in figure 2.2.
a valid solution,
. Equation (2.8)
r it also satisfies

(2.9)

ng equation and
placian in polar
converting the

(2.10)

(2.11)

ions are indeed
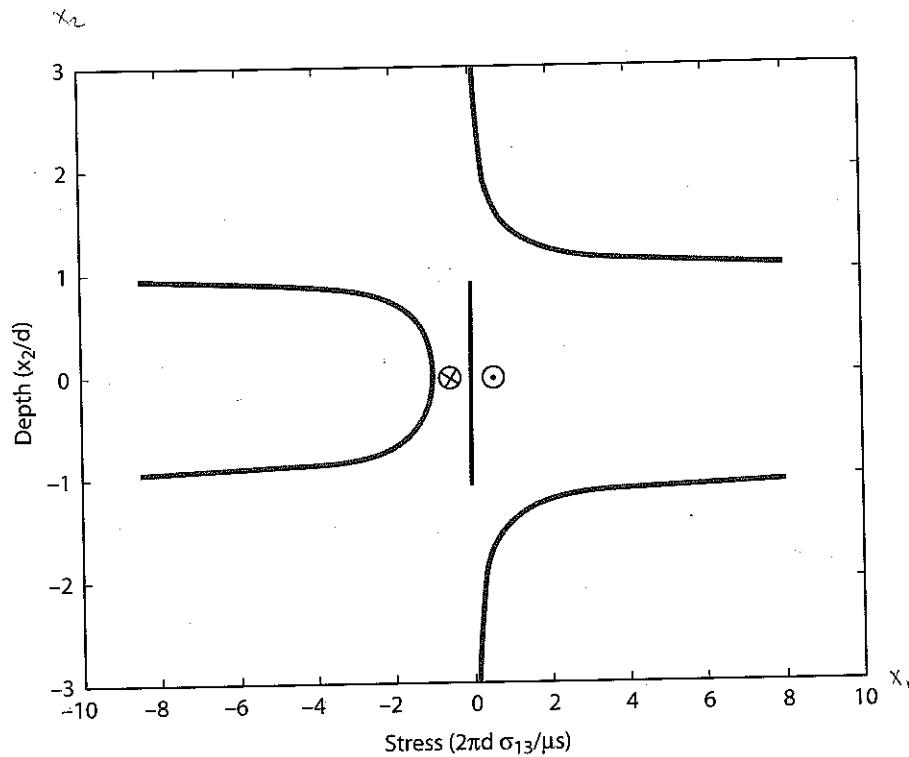
ocation surface.
es can be found

(2.12)

(2.13)

Figure 2.4. Stress change due to a pair of dislocations at $x_2 = -1$ and $x_2 = +1$.

singularity. For a finite fault represented by a pair of dislocations, the stress is singular both inside and outside the fault, as seen in figure 2.4 and equation (2.16), where $x_2 - d$ and $x_2 + d$ measure the distance from each end of the fault.

For a pair of dislocations (a dipole), representing slip over a finite interval in x_2, the far-field stress decays more rapidly with distance than it does for a single dislocation. To see this, first note that from equation (2.13), the stress resulting from a dislocation at $x_2 = -d$ is

$$\sigma_{13} = -\frac{s\mu}{2\pi} \left[\frac{x_2 + d}{x_1^2 + (x_2 + d)^2} \right]. \tag{2.17}$$

For slip due to a pair of oppositely signed dislocations, one at d and a second at slightly greater depth $d + \Delta d$, the stress is thus

$$\sigma_{13} = -\frac{s\mu}{2\pi} \left[\frac{x_2 + d + \Delta d}{x_1^2 + (x_2 + d + \Delta d)^2} - \frac{x_2 + d}{x_1^2 + (x_2 + d)^2} \right]. \tag{2.18}$$

Noticing that in the limit as $\Delta d \to 0$, this is the formal definition of a differential, we can write the stress as

$$\sigma_{13} = -\frac{s\mu\Delta d}{2\pi} \frac{\partial}{\partial d} \left[\frac{x_2 + d}{x_1^2 + (x_2 + d)^2} \right],$$

$$= -\frac{M_0}{2\pi} \frac{\cos(2\alpha)}{r^2}, \tag{2.19}$$

where M_0 is the seismic moment (see chapter 3) per unit length of fault; $M_0 = \mu s \Delta d$, the product of the shear modulus, the slip, and the fault area per unit length in the x_3
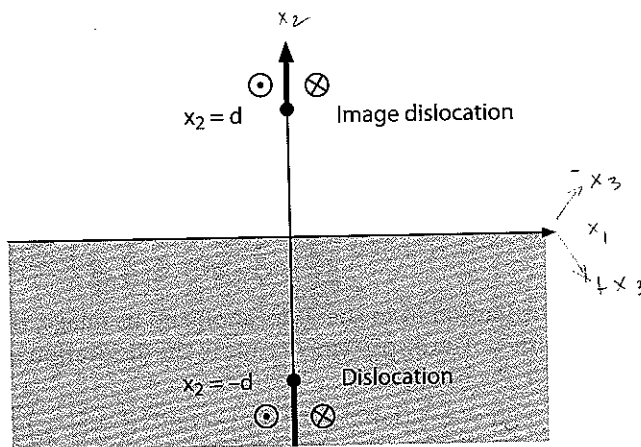
Figure 2.5. Dislocation at $x_2 = -d$, and image dislocation at $x_2 = d$.

direction; and α is the angle between the x_1 axis and the vector pointing from the center of the dislocation dipole to the observation point, as in figure 2.3. In summary, the dislocation stresses decay proportional to $1/r$ in two dimensions, and the stresses due to a dislocation dipole, in two dimensions, as $1/r^2$, as long as $r \gg \Delta d$.

2.2 Half-Space Solution

To a reasonable approximation, no stress is transmitted between the solid earth and the atmosphere. We will thus model the earth's surface as one across which the shear and normal tractions vanish. Furthermore, if all of the relevant length scales in the problem are small compared with the earth's radius, we are able to ignore earth curvature and model the free surface as planar. Here, the free surface is taken to be $x_2 = 0$, so the governing equations must be satisfied for all $x_2 < 0$. For antiplane strain problems, the half-space solution is easily constructed using the *method of images*.

What are the stresses acting on the surface $x_2 = 0$ due to a dislocation in a full-space at $x_2 = -d$? The only nonzero stress acting on the surface is σ_{23}, and from equation (2.12),

$$\sigma_{23} = \frac{s\mu}{2\pi} \frac{x_1}{x_1^2 + (x_2 + d)^2},$$ (2.20)

$$\sigma_{23}(x_2 = 0) = \frac{s\mu}{2\pi} \frac{x_1}{x_1^2 + d^2}.$$ (2.21)

Clearly, a single dislocation itself does not satisfy the free-surface boundary condition. The remedy is to add a (fictitious) image dislocation at $x_2 = d$ with opposite sign, equidistant from the putative free surface (figure 2.5). We must ensure that the image dislocation surface is restricted to the region $x_2 > 0$ so that it does not generate discontinuities within the earth ($x_2 < 0$). Note that in figure 2.5, the actual dislocation points along the negative x_2 axis. In section 2.5, you will see that changing the direction of the dislocation surface 180 degrees reverses the sense of slip, so that by comparing to figure 2.2, it is in fact the $-s$ solution that is shown in figure 2.5.

The σ_{23} stress due to the dislocation and its image is

$$\sigma_{23} = \frac{s\mu}{2\pi}\left[\frac{x_1}{x_1^2 + (x_2 + d)^2} - \frac{x_1}{x_1^2 + (x_2 - d)^2}\right],\tag{2.22}$$

so the stress on the surface $x_2 = 0$ is

$$\sigma_{23}(x_2 = 0) = \frac{s\mu}{2\pi}\left(\frac{x_1}{x_1^2 + d^2} - \frac{x_1}{x_1^2 + d^2}\right) = 0.\tag{2.23}$$

By summing the contribution from the dislocation and its image, the free-surface boundary condition is now satisfied. The displacements due to the dislocation and its image are given by

$$u_3 = \frac{-s}{2\pi}\left[\tan^{-1}\left(\frac{x_1}{x_2 + d}\right) - \tan^{-1}\left(\frac{x_1}{x_2 - d}\right)\right].\tag{2.24}$$

We can now construct a solution for slip over a finite interval in a half-space by summing the contributions from two dislocations and their respective images. In particular, assume that slip is uniform from depth d_2 to depth d_1, where $|d_1| > |d_2|$. Using the principle of superposition,

$$u_3 = \frac{-s}{2\pi}\left[\underbrace{\tan^{-1}\left(\frac{x_1}{x_2 + d_1}\right)}_{\text{deep dislocation}} - \underbrace{\tan^{-1}\left(\frac{x_1}{x_2 - d_1}\right)}_{\text{deep image}} - \underbrace{\tan^{-1}\left(\frac{x_1}{x_2 + d_2}\right)}_{\text{shallow dislocation}} + \underbrace{\tan^{-1}\left(\frac{x_1}{x_2 - d_2}\right)}_{\text{shallow image}}\right].$$

$$\tag{2.25}$$

Displacements on the free surface are of particular interest, since this is where data is collected:

$$u_3(x_2 = 0) = \frac{-s}{\pi}\left[\tan^{-1}\left(\frac{x_1}{d_1}\right) - \tan^{-1}\left(\frac{x_1}{d_2}\right)\right].\tag{2.26}$$

In the next sections, we will consider two limiting cases of this result.

2.2.1 Coseismic Faulting

Let the shallow dislocation come to the surface—that is, $d_2 \to 0$. This describes uniform slip from the surface to depth d_1 (figure 2.6). First note that

$$\lim_{d_2 \to 0}\tan^{-1}\left(\frac{x_1}{d_2}\right) = \frac{\pi}{2}\,\text{sgn}(x_1),\tag{2.27}$$

so that

$$u_3(x_2 = 0) = \frac{-s}{\pi}\left[\tan^{-1}\left(\frac{x_1}{d_1}\right) - \frac{\pi}{2}\,\text{sgn}(x_1)\right].\tag{2.28}$$

Now notice that

$$\tan^{-1}\left(\frac{x_1}{d_1}\right) + \tan^{-1}\left(\frac{d_1}{x_1}\right) = \frac{\pi}{2}\,\text{sgn}(x_1),\tag{2.29}$$

Figure 2.6
in and ou

so that

which h
cept at t
nondiffe

Note
[2.31]), i
The max
at the fa
δ tends t
of the st

2.2.2 Inter
Now let
the surf
This wa

(2.22)

(2.23)

face boundary
ge are given by

(2.24)

summing the
ssume that slip
perposition,

$$\left[\underbrace{\left(\frac{x_1}{x_2 - d_2} \right)}_{ow\ image} \right].$$

(2.25)

ta is collected:

(2.26)
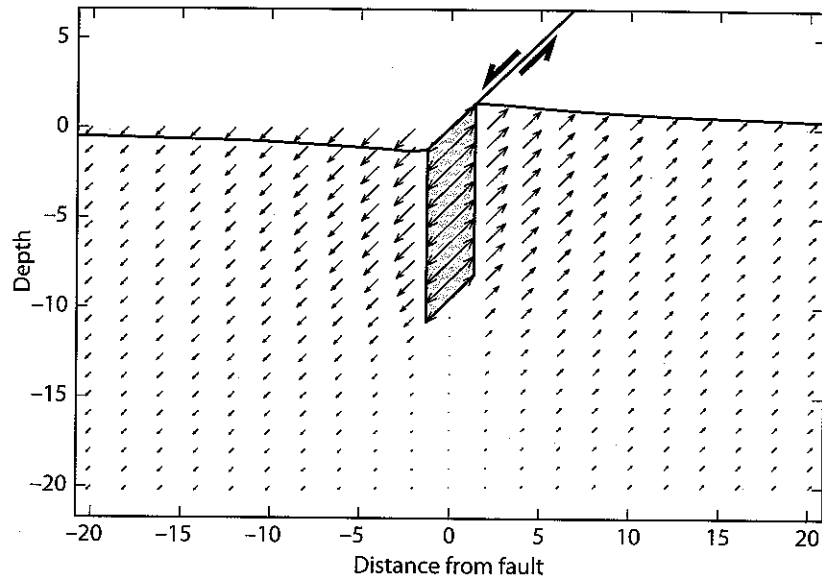
uniform slip

(2.27)

(2.28)

(2.29)

Figure 2.6. Dislocation slips from the earth's surface to depth $d_1 = 10$ km. Displacements are directed in and out of the page but are plotted to simulate a three-dimensional perspective.

so that

$$u_3(x_2 = 0) = \frac{s}{\pi} \tan^{-1} \left(\frac{d_1}{x_1} \right),$$

(2.30)

which holds for all values of x_1 (figure 2.7). We can now compute the shear strain, except at the fault trace ($x_1 = 0$), where the displacements are discontinuous and therefore nondifferentiable:

$$\epsilon_{13} = \frac{1}{2} \frac{\partial u_3}{\partial x_1} = \frac{-s}{2\pi d_1} \left[\frac{1}{1 + \left(\frac{x_1}{d_1} \right)^2} \right].$$

(2.31)

Note that the *coseismic strain*, or strain change in large strike-slip earthquakes (equation [2.31]), is everywhere negative. That is because earthquakes release shear strain, as expected. The maximum strain, which occurs at the fault trace, is $-s/2\pi d_1$. Note that the displacement at the fault trace is discontinuous, so the strain there must be defined at $x_1 = \pm\delta$ in the limit as δ tends to zero. The strain change decays with distance from the fault such that the magnitude of the strain is half the maximum when $x_1 = d_1$ (figure 2.7).

2.2.2 Interseismic Deformation

Now let the deep dislocation go to infinity, $d_1 \to \infty$. In this case, the fault is locked from the surface to depth d_2 but slips by a constant amount below that depth (figure 2.8). This was proposed by Savage and Burford (1970) as a first-order model of interseismic
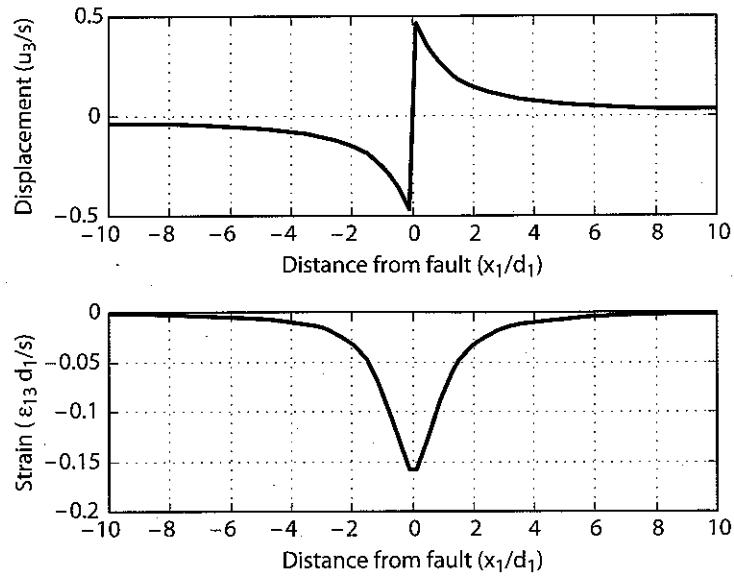
Figure 2.7. Coseismic displacement and strain.

deformation—that is, deformation between large plate rupturing events—on the San Andreas fault. In this limit, the displacement is

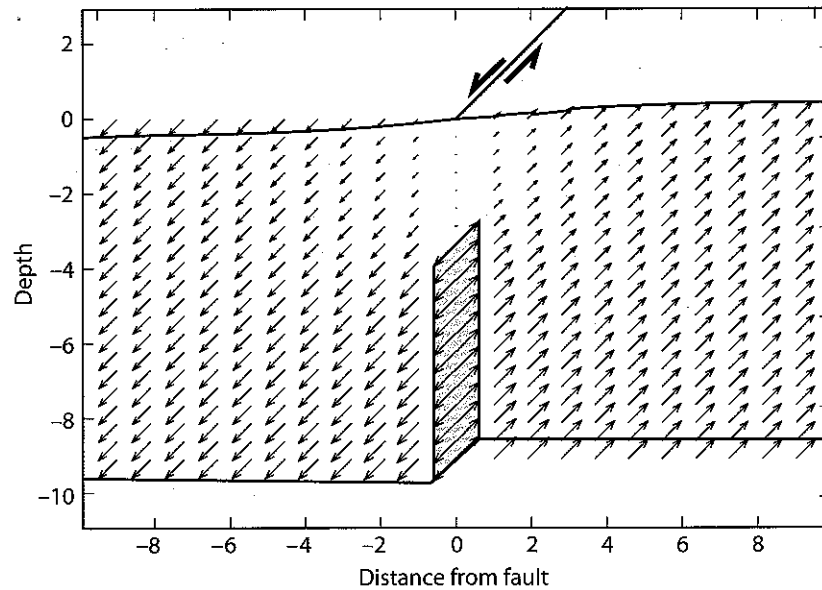$$u_3(x_2 = 0) = \frac{s}{\pi} \tan^{-1}\left(\frac{x_1}{d_2}\right). \tag{2.32}$$

Figure 2.8. Fault is locked from the earth's surface to depth $d_2 = 3$ km. Displacements are directed in and out of the page but are plotted to simulate a three-dimensional perspective.
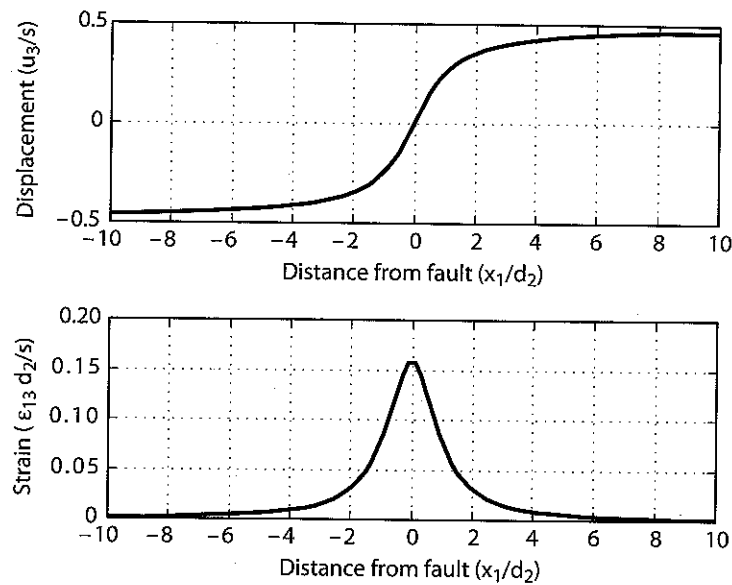
Figure 2.9. Interseismic displacement and strain.

Differentiating equation (2.32) with respect to time yields the surface velocity v_3. If the geometry is time-invariant—that is, if the depth d_2 does not change with time,

$$v_3(x_2 = 0) = \frac{\dot{s}}{\pi} \tan^{-1}\left(\frac{x_1}{d_2}\right), \tag{2.33}$$

where $\dot{s} = ds/dt$ is the fault slip rate. Note from equation (2.33) and figure 2.9 that the velocity far from the fault is equal to half the fault slip rate.

Differentiating equation (2.33) with respect to the spatial coordinate perpendicular to the fault yields the shear strain rate at the free surface:

$$\dot{\epsilon}_{13} = \frac{1}{2}\frac{\partial v_3}{\partial x_1} = \frac{\dot{s}}{2\pi d_2}\left[\frac{1}{1 + \left(\frac{x_1}{d_2}\right)^2}\right]. \tag{2.34}$$

Notice that the shear strain rate is everywhere positive; thus, shear strain accumulates on the fault between earthquakes. In fact, the *interseismic strain* (2.34) is exactly equal in magnitude and opposite in sign to the coseismic strain (2.31) if the cumulative deep slip integrated over the time between earthquakes is equal to the coseismic slip (figure 2.10). Thus, after a complete earthquake cycle, there is no strain in the intervening blocks, simply rigid block translation of the two sides of the fault.

It is important to note that, as mentioned earlier, the deformation is caused by the dislocation line and not by the dislocation surface. The implication of this is that the deformation field at the surface is independent of the dip of the fault, if the slip on the fault is spatially
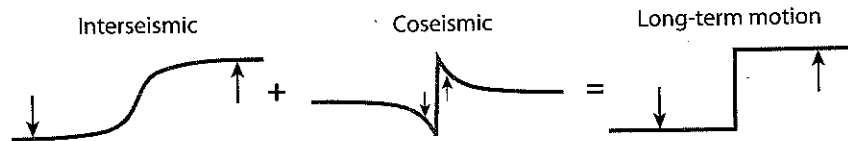
Figure 2.10. Interseismic displacement plus coseismic displacement equals the long-term fault motion.
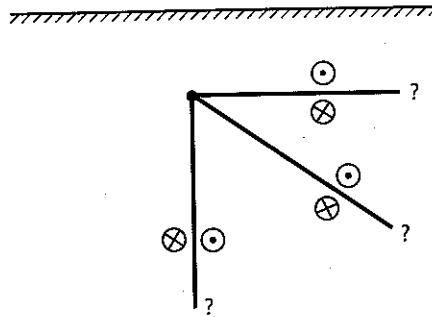

Figure 2.11. The surface displacements and strain are independent of the dip of the dislocation surface for a single screw dislocation.

uniform and extends to infinite depth, as long as the fault does not breach the surface. In particular, the deformation at the surface is the same whether the fault plane is vertical (as we have modeled it) or horizontal. A horizontal dislocation might represent a zone of decoupling. Our results show, unfortunately, that we cannot distinguish between these models on the basis of surface displacement or strain for infinitely long strike-slip faults (figure 2.11).

There is an alternative perspective on interseismic deformation that is commonly used in both elastic and viscoelastic models. One can consider that over the long term, the fault moves in essentially rigid block motion, with no strain outside a narrow fault zone. Between large earthquakes, the upper part of the fault is locked. Kinematically, this can be accomplished by starting with rigid block motion and superimposing *back slip* at a rate equal to the long-term slip rate on the seismogenic part of the fault. From equation (2.30), the velocity is thus

$$v_3(x_2 = 0) = \frac{\dot{s}}{2}\, \text{sgn}(x_1) - \frac{\dot{s}}{\pi}\, \tan^{-1}\left(\frac{d}{x_1}\right),$$

$$= \frac{\dot{s}}{\pi}\, \tan^{-1}\left(\frac{x_1}{d}\right), \tag{2.35}$$

using the identity in equation (2.29). The back-slip model yields the same result for the interseismic velocity derived previously (2.33) for a steadily creeping dislocation extending infinitely below locking depth d.

2.2.3 Postseismic Slip

Last, consider buried slip with $d_1 > d_2$. Thatcher (1975) modeled postseismic deformation along the San Andreas fault assuming slip over a confined interval beneath the coseismic rupture surface. During an earthquake, stress decreases along the slipping fault and is shed to the lower part of the fault. If the fault in the lower crust creeps in response to the imposed stress, there may be transient buried slip. This model is a very simple representation of that process. More realistic models, which account for stress-driven frictional creep or distributed
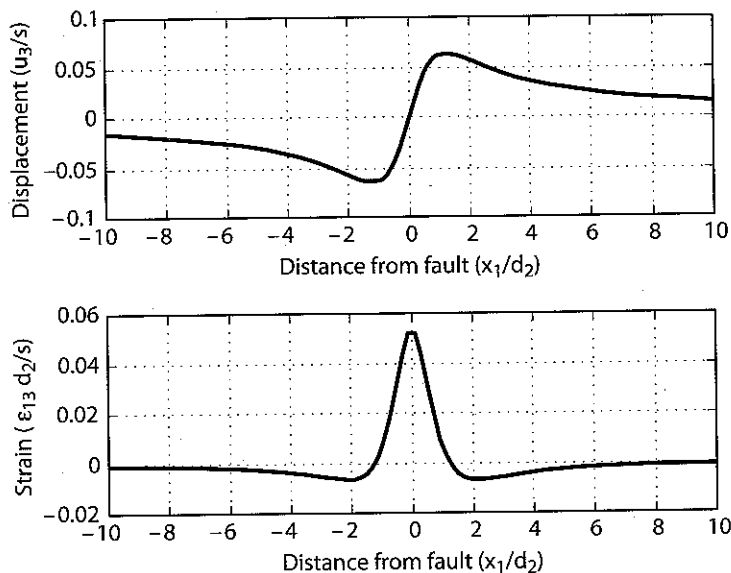
Figure 2.12. Postseismic displacement and strain.

viscoelastic deformation, will be considered in later chapters. This present model is useful primarily because of its simplicity.

For confined slip between depths d_1 and d_2, the displacements at the free surface are

$$u_3(x_2 = 0) = \frac{-s}{\pi} \left[\tan^{-1} \left(\frac{x_1}{d_1} \right) - \tan^{-1} \left(\frac{x_1}{d_2} \right) \right],$$ (2.36)

while the surface strains are

$$\epsilon_{13} = \frac{s}{2\pi} \left(\frac{d_2}{d_2^2 + x_1^2} - \frac{d_1}{d_1^2 + x_1^2} \right).$$ (2.37)

Note that the strain, for buried slip, undergoes a sign change (figure 2.12), being positive near the fault and negative away from the fault. This feature turns out to be characteristic of deformation occurring over a finite depth interval. It is common to more sophisticated and realistic models of postseismic deformation.

2.3 Distributed Slip

We can use the results in the previous section to derive a general expression for deformation due to an arbitrary distribution of fault slip with depth. Consider the case where slip is confined to the interval from d to $d + \Delta d$:

$$u_3(x_2 = 0) = \frac{-s}{\pi} \left[\tan^{-1} \left(\frac{x_1}{d + \Delta d} \right) - \tan^{-1} \left(\frac{x_1}{d} \right) \right].$$ (2.38)
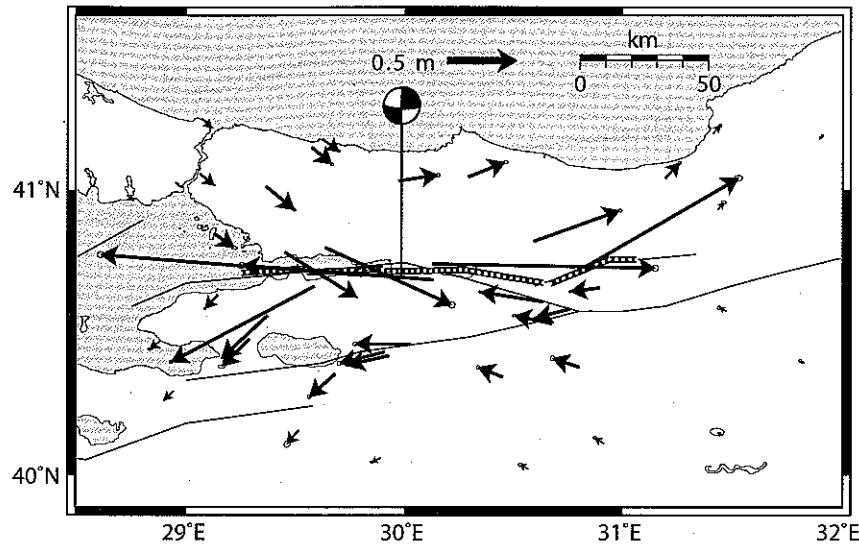
Figure 2.13. Horizontal components of the coseismic displacements during the 17 August 1999 Izmit, Turkey, earthquake. Dashed line indicates the rupture zone of the earthquake. Data from Reilinger et al. (2000).

Noticing that in the limit as $\Delta d \to 0$, this is the formal definition of a differential, we can write the displacement due to slip over Δd as

$$u_3(x_1, x_2 = 0) = \frac{-s\Delta d}{\pi} \frac{\partial}{\partial d} \tan^{-1}\left(\frac{x_1}{d}\right), \tag{2.39}$$

$$= \frac{s\Delta d}{\pi} \frac{x_1}{x_1^2 + d^2}. \tag{2.40}$$

Thus, the displacement due to an arbitrary distribution of slip with depth, $s(\xi)$, is

$$u_3(x_1, x_2 = 0) = \frac{1}{\pi} \int_0^\infty s(\xi) \frac{x_1}{x_1^2 + \xi^2} d\xi. \tag{2.41}$$

The forward problem, predicting the surface displacements at x_1 given the slip distribution $s(\xi)$, is solved simply by integrating. Commonly, we have measured displacements at the earth's surface and want to determine as much as possible about the distribution of slip at depth in the earth. This inverse problem, estimating $s(\xi)$ from measured values of $u_3(x_1, x_2 = 0)$, was addressed by Matthews and Segall (1993) among others.

2.4 Application to the San Andreas and Other Strike-Slip Faults
The simple models explored in this chapter can be compared to actual displacements recorded in large strike-slip earthquakes. Displacements during the 17 August 1999, Izmit, Turkey, earthquake, a magnitude 7.5 event, were precisely measured using Global Positioning System (GPS) receivers. The horizontal components of the displacements during the earthquake are shown in figure 2.13. The earthquake rupture was approximately 150 km long, hardly infinite. However, if we focus on measurements made near the central part of the east–west trending rupture, end effects can be minimized.
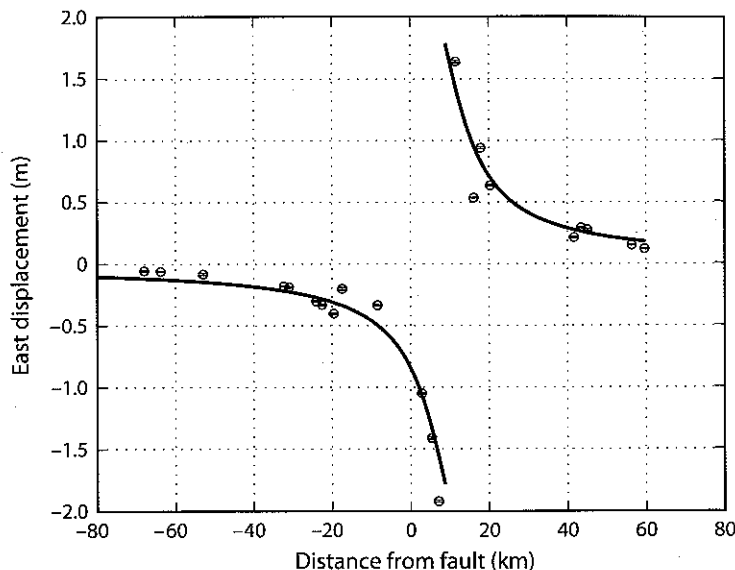
Figure 2.14. Coseismic displacements during the 17 August 1999 Izmit, Turkey, earthquake. Data from Reilinger et al. (2000). The fault parallel (east–west) component of the displacement is plotted as a function of (north–south) distance perpendicular to the fault. Only stations near the middle of the rupture are plotted to minimize effects of the fault ends. Also shown is the prediction of the simple infinitely long screw dislocation equation (2.30), with slip of 3.6 m and a fault depth of 8 km.

Figure 2.14 shows the fault-parallel (east–west) displacements as a function of north–south distance perpendicular to the fault. Also shown is the prediction from a simple two-dimensional screw dislocation extending from the earth's surface to a depth of 8 km with 3.6 m of slip. It is quite remarkable that this exceedingly simple model fits the data so well. A three-dimensional model is required to fit the observations more accurately. Inversions of the GPS measurements, which allow the slip to vary in magnitude over the fault plane, yield a maximum slip of 5.7 m and an average slip of 3.6 m over the central 75 km of the rupture (Reilinger et al. 2000).

We can also use the results of this chapter to estimate the interseismic slip rate on the San Andreas fault and the depth to which the fault is locked between earthquakes—the so-called *locking depth*. A summary of strain-rate data shown in Figure 2.15, from Thatcher (1990), shows a broad zone of shearing centered on the San Andreas fault. We can interpret the data using the simple model of a single-screw dislocation slipping at a constant rate given in equation (2.34). This equation shows that the shear strain drops to half its peak value at a distance d from the fault. From the figure, we estimate that half-width to be approximately 30 km. Given this, the interseismic slip rate $\dot{s}$ is given by

$$\dot{s} = \pi d (2\dot{\epsilon}_{13})_{max}. \tag{2.42}$$

The data show a maximum engineering shear strain rate, $(2\dot{\epsilon}_{13})_{max}$, of approximately 5×10^{-7} 1/yr. This leads to a slip rate of roughly 4.7 cm/yr.

These estimates are higher than our best current estimates. The main reason is that, in most places in California, there is not a single fault but multiple parallel faults. This causes the strain to be spread out over a broader area than would be predicted from a single dislocation
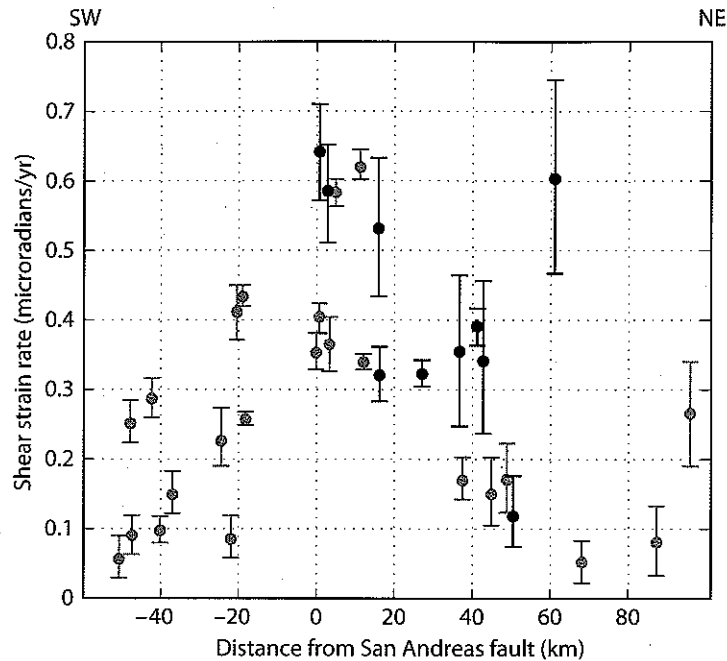
Figure 2.15. Shear strain rate as a function of distance from the San Andreas fault. In this figure, the strain rate is given in engineering strain, which is twice the tensor strain used in this text. (Light symbols, southern California, dark symbols, northern California.) After Thatcher (1990).
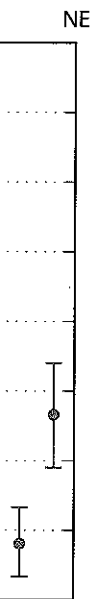
and biases to large values the locking depth. Overestimating d also causes the slip rate to be overestimated.

The slip rate $\dot{s}$ is estimated to be closer to 3.5 cm/yr, from both geologic and geodetic studies in the central creeping section of the San Andreas. With this slip rate and the observed maximum shear strain rate of 5×10^{-7} 1/yr, we estimate d to be approximately 20 km.

One can do a better job by considering measurements from a more limited geographic region. The Southern California Earthquake Center (SCEC) has produced a crustal velocity field using GPS, Very Long Baseline Interferometry (VLBI), and Electronic Distance Meter (EDM) measurements. The GPS data span the time interval 1986 to 1997 and consist of a mixture of episodic campaign measurements and continuously recording stations. VLBI measurements at 10 southern California sites were collected between 1980 and 1994, whereas the EDM surveys were conducted predominantly from 1970 to 1992.

In order to isolate a relatively simple part of the San Andreas fault system, we focus on data from the Carrizo Plain section, north of the Big Bend in the San Andreas (figure 2.16). In this region, the San Andreas fault trace is relatively straight and simple. Also the area is not complicated by additional faults, except perhaps in the Santa Maria basin. The velocity vectors, which are displayed in a North America fixed reference frame, are very nearly parallel to the San Andreas and increase in magnitude from east to west.

In order to model these velocities, we need to account for the fact that the data and model are in different reference frames. The data are in a North America fixed frame; sites on stable North America are expected to have zero motion. The model given by equation (2.33), however, predicts half the motion on one side of the fault, and half on the other side. By symmetry, the fault trace has zero velocity. One must account for this difference in comparing the model predictions to measured velocities.
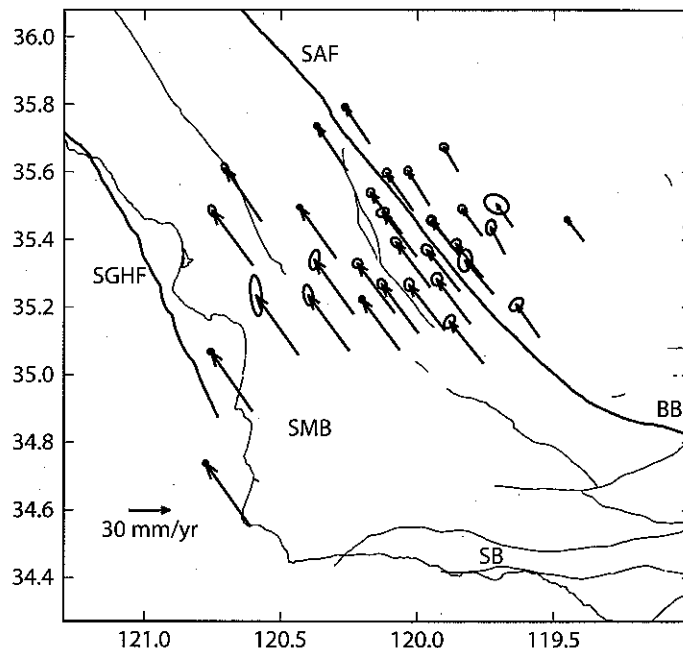
NE

Figure 2.16. Interseismic station velocities relative to stable North America from the 1980s and 1990s as measured by a variety of techniques, analyzed and compiled by the Southern California Earthquake Center. SAF = San Andreas fault; SGHF = San Gregorio Hosgri fault; BB = Big Bend of San Andreas; SMB = Santa Maria basin; SB = Santa Barbara.

fault. In this figure, the this text. (Light symbols,

uses the slip rate to be

geologic and geodetic rate and the observed mately 20 km.
re limited geographic ced a crustal velocity ronic Distance Meter 1997 and consist of ording stations. VLBI 80 and 1994, whereas

system, we focus on Andreas (figure 2.16). mple. Also the area is ia basin. The velocity re very nearly parallel

ct that the data and a fixed frame; sites on n by equation (2.33), on the other side. By fference in comparing

Figure 2.17 shows a profile of the fault-parallel component of velocity perpendicular to the trend of the San Andreas fault. The San Andreas is located at $x = 0$. Also shown is the theoretical prediction from equation (2.33) for a fault-locking depth of 20 km and a slip rate of 39.5 mm/yr. While there are significant misfits at points farthest from the fault, the comparison between the observations and the prediction of the simple model is satisfactory. Discrepancies could result from larger than expected observational errors or defects in the model, such as additional deformation sources, nonuniform elastic properties, or complexities in fault geometry, to name a few. We will revisit these data in chapter 12 in the context of viscoelastic earthquake cycle models. With these models, the surface velocity field can be fit with slip rates consistent with paleoseismic observations and locking depths consistent with the depths of major strike-slip earthquakes in California.

2.5 Displacement at Depth
The displacements within the earth can be computed from equation (2.25). Care must be taken when evaluating the $\tan^{-1}$ functions because they are discontinuous. Mathematically, the discontinuities are referred to as *branch cuts*. We must ensure that the branch cuts occur on the fault surface and not elsewhere.

First, recall that figure 2.2 defined the dislocation to extend along the positive x_2 axis, with the angle θ measured positive clockwise from x_2. Looking from above the fault, the $+s\theta/2\pi$ solution is left-lateral, with the negative x_1 side moving in the positive x_3 direction. Add a right-lateral rigid body offset along the fault with slip that exactly negates the slip due to the dislocation for $x_2 > 0$ (figure 2.18). The sum is a right-lateral dislocation that extends along the
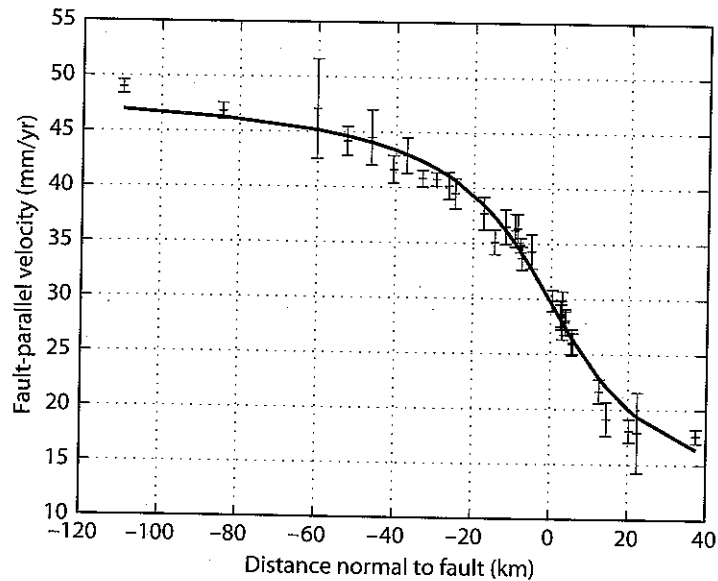
Figure 2.17. Velocity profile across the San Andreas fault. Fault-parallel component of velocity for the stations shown in figure 2.16. Error bars are one standard deviation. The San Andreas fault is approximately located at $x = 0$. Also shown is the predicted velocity of an infinitely long buried screw dislocation from equation (2.33) for a fault-locking depth of 20 km and a slip rate of 39.5 mm/yr.
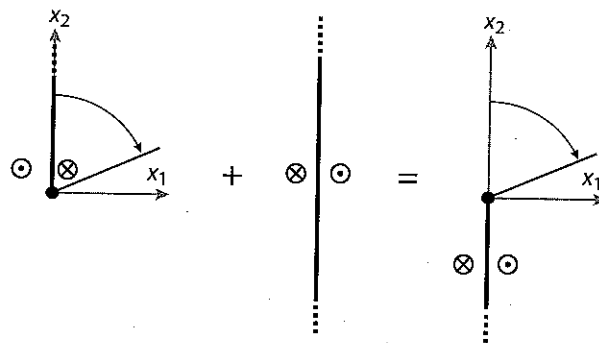

Figure 2.18. Definition of branch cuts for a strike-slip fault. Figure on the left shows the dislocation extending along the positive x_2 axis. Addition of rigid body slip of opposite sign cancels the slip in the domain $x_2 > 0$ and generates an oppositely signed dislocation for $x_2 < 0$.

negative x_2 axis. Thus, flipping the dislocation plane 180 degrees changes the sense of slip on the fault. For example, for a buried dislocation extending in the negative x_2 direction, its image dislocation extending in the positive x_2 direction, as in figure 2.5, has the *same* sense of slip, since changing the orientation of the plane 180 degrees is equivalent to changing the sense of slip.

For the dislocation extending along the negative x_2 direction, the branch cut is located at $\theta = \pi$, so we must define the argument of the function θ to be $-\pi < \theta < \pi$. Figure 2.19 shows the branch cuts for a buried dislocation between depths d_1 and d_2. Numerical calculations that compute the displacements in the body should use an arctangent function that takes two arguments and produces the correct sign to represent an angle in each of the four quadrants.
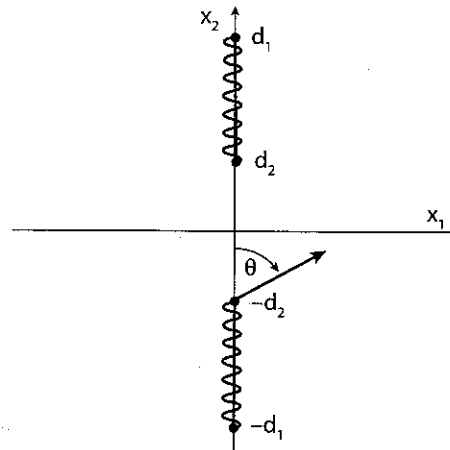
Figure 2.19. Definition of branch cuts (wavy lines) for a strike-slip fault in a half-plane.

Figures 2.6 and 2.8 show the displacement field for uniform-slip dislocations. Notice that the displacements decay quite rapidly below the dislocation and with distance away from the dislocation.

2.6 Summary and Perspective

It is worth reviewing the approach and assumptions made in this chapter. We assumed that the earth could be modeled as a homogeneous, isotropic, elastic half-space. Our simple fault model involved specifying the displacement on the fault surface. For two-dimensional antiplane geometry, as might approximate a very long strike-slip fault, we found that the displacements must satisfy Laplace's equation. Solutions in a full-space are easily constructed, and half-space solutions are then found using the method of images. The displacements at the free surface are found to follow the familiar $\tan^{-1}$ distribution, with argument either x/d or d/x, depending on whether the fault is locked or slipping at the earth's surface.

The limitations to these simple models are manifold. The main benefits of the results developed in this chapter are their simplicity and the fact that to first order, they fit some geodetic observations quite well. However, faults are never infinitely long, and we may be very interested in effects near the end of an earthquake rupture. Three-dimensional dislocations will be the subject of chapter 3. Furthermore, we have so far ignored the earth's curvature and topography; this will be considered in chapter 8. The earth is not homogeneous and isotropic, nor perfectly elastic, for that matter. Methods for determining elastic fields due to dislocations in heterogeneous earth models are discussed in chapter 5. The effects of viscoelastic relaxation are described in chapter 6. Last, we should note that by specifying the fault slip, we are unable to say anything about *how* that slip comes about. A more complete description of faulting involves specifying a constitutive law for the fault surface, or fault zone, and then computing how the slip develops as a function of time for some loading geometry (as in chapter 11). As a first step in that direction, we will consider crack models in which the stress change (stress drop) on the fault surface is specified in chapter 4.

In the next chapter, we will begin by deriving dislocation solutions for two-dimensional dip-slip faults and faults in three dimensions.

2.7 Problems

1. Show that the stress due to a pair of screw dislocations is proportional to $\cos(2\theta)/r^2$, as in equation (2.19).

2. Use the principle of superposition to derive expressions for the surface velocity and strain rate for two parallel faults that are locked from the earth's surface to some depth d. The first fault is located at $x_1 = \zeta_1$ and has slip rate $\dot{s}_1$, and the second fault is located at $x_1 = \zeta_2$, with slip-rate $\dot{s}_2$. Generalize this to an arbitrary number of faults. This simple model can be compared to geodetic measurements collected across the San Andreas fault system in northern California.

3. Show that the surface displacements for a slip distribution that varies linearly with depth as $s(\xi) = s_0(1 - \xi/D)$ are given by

$$u_3(x_1, x_2 = 0) = \frac{s_0}{\pi} \left[\tan^{-1}\left(\frac{D}{x_1}\right) - \frac{x_1}{2D} \log\left(\frac{D^2 + x_1^2}{x_1^2}\right) \right]. \tag{2.43}$$

4. Prove that for a single screw dislocation buried in an elastic half-space that does not cut the free surface, the displacement field at the free surface is independent of the dip of the dislocation plane (see figure 2.11).

5. Write a script to plot the interseismic displacements within the earth due to an infinitely long, buried nonvertical strike-slip fault. Include the contributions from the image sources so that the plane $x_2 = 0$ is traction free.

2.8 References

Matthews, M. V., and P. Segall. 1993. Statistical inversion of crustal deformation data and estimation of the depth distribution of slip in the 1906 earthquake. *Journal of Geophysical Research* **98**, 12,153–12,163.

Reilinger, R. E., S. Ergintav, R. Bürgmann, S. McClusky, O. Lenk, A. Barka, O. Gurkan, L. Hearn, K. L. Feigl, R. Cakmak, B. Aktug, H. Ozener, and M. N. Töksoz. 2000. Coseismic and postseismic fault slip for the 17 August 1999, M = 7.5, Izmit, Turkey, earthquake. *Science* **289**, 1519–1524.

Savage, J. C., and R. O. Burford. 1970. Accumulation of tectonic strain in California. *Bulletin of the Seismological Society of America* **60** (6), 1877–1896.

Thatcher, W. 1975. Strain accumulation and release mechanism of the 1906 San Francisco earthquake. *Journal of Geophysical Research* **80**, 4862–4872.

———. 1990. Present-day crustal movements and the mechanics of cyclic deformation. In R. E. Wallace, Ed., *The San Andreas Fault system*, U.S. Geological Survey Professional Paper 1515. Washington, DC: U.S. Government Printing Office, pp. 189–205.